Monthly Notices of the ROYAL ASTRONOMICAL SOCIETY

MNRAS **513,** 282–295 (2022) https://doi.org/10.1093/mnras/stac895
Advance Access publication 2022 April 13

Numerical study of cosmic ray confinement through dust resonant drag instabilities

Suoqing Ji(季索清) [1,2★] Jonathan Squire [3] and Philip F. Hopkins [2]

[1]*Astrophysics Division & Key Laboratory for Research in Galaxies and Cosmology, Shanghai Astronomical Observatory, Chinese Academy of Sciences, Shanghai 200030, China*
[2]*TAPIR & Walter Burke Institute for Theoretical Physics, Mailcode 350-17, California Institute of Technology, Pasadena, CA 91125, USA*
[3]*Physics Department, University of Otago, 730 Cumberland St., Dunedin 9016, New Zealand*

Accepted 2022 March 29. Received 2022 March 10; in original form 2021 November 29

ABSTRACT

We investigate the possibility of cosmic ray (CR) confinement by charged dust grains through resonant drag instabilities (RDIs). We perform magnetohydrodynamic particle-in-cell simulations of magnetized gas mixed with charged dust and cosmic rays, with the gyro-radii of dust and GeV CRs on ∼au scales fully resolved. As a first study, we focus on one type of RDI wherein charged grains drift super-Alfvénically, with Lorentz forces strongly dominating over drag forces. Dust grains are unstable to the RDIs and form concentrated columns and sheets, whose scale grows until saturating at the simulation box size. Initially perfectly streaming CRs are strongly scattered by RDI-excited Alfvén waves, with the growth rate of the CR perpendicular velocity components equaling the growth rate of magnetic field perturbations. These rates are well-predicted by analytic linear theory. CRs finally become isotropized and drift at least at $\sim v_{\rm A}$ by unidirectional Alfvén waves excited by the RDIs, with a uniform distribution of the pitch angle cosine μ and a flat profile of the CR pitch angle diffusion coefficient $D_{\mu\mu}$ around $\mu = 0$, without the '90° pitch angle problem.' With CR feedback on the gas included, $D_{\mu\mu}$ decreases by a factor of a few, indicating a lower CR scattering rate, because the backreaction on the RDI from the CR pressure adds extra wave damping, leading to lower quasi-steady-state scattering rates. Our study demonstrates that the dust-induced CR confinement can be very important under certain conditions, e.g. the dusty circumgalactic medium around quasars or superluminous galaxies.

Key words: MHD – plasmas – methods: numerical – cosmic rays – ISM: structure – galaxies: active.

1 INTRODUCTION

The transport physics of cosmic rays (CRs) has been a subject of active investigation since the 1960s (Kulsrud & Pearce 1969). As charged ultrarelativistic particles coupled to magnetic fields via Lorentz forces, CRs are fundamentally governed by particle-wave-interactions with magnetic fluctuations (e.g. Alfvén waves). Generally speaking, when Alfvén waves are excited with wavelengths broadly similar to the CR gyro radii, CRs are scattered towards isotropy in the wave frame from small-scale irregularities of field lines and thus become 'confined' (the net drift/streaming speed relative to the plasma is suppressed). The relevant confining Alfvén waves can be excited by the CR streaming instability when the CR drift velocity v_D exceeds local Alfvén velocity $v_{\rm A} \equiv |\boldsymbol{B}|/\sqrt{4\pi\rho_{\rm gas}}$ (Kulsrud & Pearce 1969), and/or by extrinsic turbulence (Jokipii 1966; Skilling 1971). On the other hand, CRs are less confined when Alfvén waves are strongly damped, via ion-neutral damping, non-linear Landau damping (Lee & Völk 1973) or through the magnetohydrodynamic (MHD) turbulence cascade (Yan & Lazarian 2002; Farmer & Goldreich 2004). Therefore, studying the excitation and damping mechanisms of Alfvén waves around these gyro-resonant scales is crucial to understanding of CR transport.

Recently, a number of numerical studies have attempted to model the effects of CRs around energies of ∼GeV (which dominate the CR energy density) on ISM and galactic scales. These studies suggest that CRs can have a significant influence on galactic 'feedback processes' regulating star and galaxy formation (e.g. Pakmor et al. 2016; Ruszkowski, Yang & Zweibel 2017; Farber et al. 2018; Chan et al. 2019; Hopkins et al. 2020; Buck et al. 2020; Su et al. 2020) and the phase structure and nature of the circumgalactic medium (CGM; e.g. Salem, Bryan & Corlies 2016; Butsky & Quinn 2018; Ji et al. 2020, 2021). Meanwhile, classical models of Galactic CR transport which compare to Solar system CR experiments (Strong & Moskalenko 2001; Jóhannesson et al. 2016; Evoli et al. 2017) have suggested the potential for new breakthroughs in particle physics from detailed modeling of ratios of e.g. secondary-to-primary ratios in CR populations. However, in all of these studies a fluid or Fokker–Planck description of CR transport is required, usually with some simple assumption that CRs have a constant 'diffusion coefficient' or 'streaming speed' or effective scattering rate. But this introduces significant uncertainties, as the microphysical behaviour and even the qualitative physical origin of these scattering rates (and therefore their dependence on plasma properties) remains deeply uncertain. This uncertainty is vividly demonstrated in Hopkins et al. (2021b):

★ E-mail: suoqing@shao.ac.cn

comparing different CR transport scalings based on local plasma properties according to different proposed scattering-rate models in the literature, Hopkins et al. (2020b) showed that existing models could (1) differ by factors larger than $\sim 10^6$ in their predicted effective transport coefficients, and (2) even models with similar mean diffusion coefficients could produce (as a consequence of different detailed dependence on plasma properties) qualitatively different CR transport outcomes and effects on ISM and CGM properties. Therefore, it is particularly important to go beyond simple fluid treatments of CRs by investigating explicit CR scattering physics and dynamics on the scales of the CR gyroradius $r_{\rm gyro,\,cr}$ ($\sim$au for GeV CRs in typical Solar-neighbourhood ISM conditions), where the interaction between CRs and magnetic fluctuations can be fully resolved.

One potentially important piece of physics on these scales, which has been almost entirely neglected in the historical CR literature, is the role of dust grains. Recently, Squire et al. (2021) noted a remarkable coincidence: under a broad range of ISM conditions, the gyroradii of charged dust grains in the ISM (with sizes $\sim 10^{-3}$–1 μm) and $\sim$0.1–10 GeV CRs overlap. While the grains have much lower charge-to-mass ratios, they also have much lower velocities, giving nearly coincident gyro radii. As a result, Squire et al. (2021) proposed that dust grains can influence $\sim$GeV CR transport on gyro-resonant ($\sim$au) scales in two ways: (1) as inertial particles, dust can damp parallel Alfvén waves excited by the CR streaming instability and thus reduce CR confinement, and (2) dust can be unstable to the so-called 'resonant drag instabilities' (RDIs; Squire & Hopkins 2018), a recently discovered, formally infinitely large family of instabilities that appear in different forms, whenever dust grains move through a background fluid with some non-vanishing difference in the force acting on dust versus fluid. The RDIs can excite small-scale parallel Alfvén waves in magnetized gas (Hopkins & Squire 2018; Seligman, Hopkins & Squire 2019), which can in turn scatter CRs and enhance their confinement. Which of these is the dominant process, or whether still different forms of the RDIs can be excited, depend on the local plasma conditions, with scenario(s) being more likely in regions where the gas is relatively diffuse and external acceleration of dust grains is relatively strong (from e.g. absorbed photon momentum around a bright source). In any case, the co-existence of CRs and charged dust grains in the ISM is self-evident. Even in the CGM far from galaxies, where Squire et al. (2021) suggest scenario (2) would be more likely, the existence of significant dust populations is theoretically and observationally plausible: for instance, in the cool ($\sim 10^4$–10^5 K) or warm–hot (10^5–10^6 K) phases of the CGM where the gas number density is low enough ($\lesssim 10^{-3}\,{\rm cm}^{-2}$), the hadronic and Coulomb losses of CRs are small (Guo & Oh 2008), and the temperature and density are low enough that the dust sputtering time is long (Tielens et al. 1994). In fact, a significant amount of dust has already been observed in the CGM (Ménard et al. 2010; Peek, Ménard & Corrales 2015). And around quasars or superluminous galaxies, dust grains could in principle easily be accelerated by radiation pressure and become unstable to the specific RDIs which would source strong CR scattering on $\sim$au scales according to Squire et al. (2021). Dust clumping can scatter and re-emit photons from QSOs (e.g. Hennawi et al. 2010; Martin et al. 2010), and thus might produce observables in absorption lines of the CGM. Nevertheless, this scenario remains largely unexplored; even for the pure dust RDIs without CRs, the only simulation study thus far, in Hopkins, Squire & Seligman (2020), has simulated the CGM cases at a resolution of $\sim$10 pc, far above au scales on which CR-dust coupling occurs.

Motivated by the above, in this paper we present the very first numerical study of CR-dust-MHD coupling, with resolved CR and dust gyro-radii. In particular, here we focus on the proposed CR confinement scenario in which CRs are scattered by magnetic field irregularities caused by the specific forms the RDI described in Squire et al. (2021). The paper is organized as follows. In Section 2, we describe the numerical methods and setup of our simulations. Section 3 presents and analyses the simulation results. We finally summarize our findings in Section 4.

2 METHODS AND SIMULATION SETUP

2.1 Numerical methods

The numerical methods adopted here consist of three main components, each of which has been well-studied separately: the MHD solver in the code GIZMO (Hopkins 2015), dust grains evolved with a standard superparticle method (Hopkins & Squire 2018; Seligman et al. 2019), and CR particles evolved with a hybrid MHD particle-in-cell (MHD-PIC) method (Bai et al. 2015, 2019). Detailed implementations are described in the above-cited references, and we only briefly review them here.

The background plasma/fluid/gas and magnetic fields follow the equations of ideal MHD, solved in GIZMO with the well-tested constrained-gradient meshless finite-volume Lagrangian Godunov method (Hopkins 2016; Hopkins & Raives 2016). This has been shown to accurately reproduce a variety of detailed MHD phenomena including amplification, shocks, detailed structure of the magnetorotational and magnetothermal instabilities, and more (Hopkins 2017; Deng et al. 2019; Grudić et al. 2021). To this we add the 'back-reaction' or feedback force of CRs and dust on gas, detailed below. Individual grains and CRs are integrated as PIC-like 'superparticles' as is standard in the literature for both (Carballido, Stone & Turner 2008; Johansen, Youdin & Mac Low 2009; Bai & Stone 2010; Pan et al. 2011; Bai et al. 2015, 2019; McKinnon et al. 2018; Holcomb & Spitkovsky 2019; van Marle, Casse & Marcowith 2019), sampling the distribution function statistically by taking each superparticle to represent an ensemble of identical micro-particles (individual grains or CRs). Dust grains obey the equation of motion

$$\frac{d\boldsymbol{v}_{\rm dust}}{dt} = \boldsymbol{a}_{\rm ext,dust} + \boldsymbol{a}_{\rm gas,dust}, \tag{1}$$

where $\boldsymbol{v}_{\rm dust}$ is the grain velocity, $\boldsymbol{a}_{\rm ext,dust}$ and $\boldsymbol{a}_{\rm gas,dust}$ are grain accelerations from external forces (e.g. gravity and radiation) and background gas and magnetic fields, respectively. The latter includes both drag and Lorentz forces:

$$\boldsymbol{a}_{\rm gas,dust} = -\frac{\boldsymbol{v}_{\rm dust}-\boldsymbol{v}_{\rm gas}}{t_{s,\rm dust}} - \frac{\left(\boldsymbol{v}_{\rm dust}-\boldsymbol{v}_{\rm gas}\right)\times\hat{\boldsymbol{B}}}{t_{L,\rm dust}}, \tag{2}$$

where $\hat{\boldsymbol{B}} = \boldsymbol{B}/|\boldsymbol{B}|$ is the unit vector of the magnetic field $\boldsymbol{B}$, $t_{s,\,\rm dust}$ the dust drag drag or stopping time and $t_{L,\,\rm dust}$ the dust Larmor or gyro time. Since we are interested in regimes with supersonic drift and microscopic dust grains (the Epstein drag limit), the drag and gyro time-scales are given by

$$t_{s,\rm dust} \equiv \sqrt{\frac{\pi\gamma}{8}}\frac{\rho^i_{\rm dust}}{\rho_{\rm gas}}\frac{\epsilon_d}{c_s}\left(1+\frac{9\pi\gamma}{128}\frac{\left|\boldsymbol{v}_{\rm dust}-\boldsymbol{v}_{\rm gas}\right|^2}{c_s^2}\right)^{-1/2} \tag{3}$$

$$t_{L,\rm dust} \equiv \frac{m_{\rm dust}c}{q_{\rm dust}\boldsymbol{B}} = \frac{4\pi\rho^i_{\rm dust}\epsilon^3_{\rm dust}c}{3e\,|Z_{\rm dust}\boldsymbol{B}|}, \tag{4}$$

where γ is the usual adiabatic index of the gas, and $\rho^i_{\rm dust}$, $\epsilon_{\rm dust}$, $m_{\rm dust}$, and $q_{\rm dust} \equiv Z_{\rm dust}e$ are the internal density, radius, mass, and charge of dust grains, respectively.

Similarly, the equation of motion for CRs is:

$$\left(\frac{c}{\tilde{c}}\right)\frac{d\boldsymbol{u}_{\rm cr}}{dt} = \boldsymbol{a}_{\rm ext,cr} + \boldsymbol{a}_{\rm gas,cr} = \boldsymbol{a}_{\rm ext,cr} + \frac{\left(\boldsymbol{v}_{\rm cr} - \boldsymbol{v}_{\rm gas}\right)\times\hat{\boldsymbol{B}}}{t_{L,0,\rm cr}}, \tag{5}$$

where c is the speed of light (and see below for $\tilde{c}$), and $\boldsymbol{v}_{\rm cr}$ is the velocity of the CR particles, which is related to the CR four-velocity $\boldsymbol{u}_{\rm cr} \equiv \gamma_L \boldsymbol{v}_{\rm cr}$ via the usual Lorentz factor $\gamma_L \equiv (1 - |\boldsymbol{v}_{\rm cr}|^2/c^2)^{-1/2}$. The $t_{L,0,\rm cr} \equiv 1/\Omega_{\rm cr,0}$ is the usual non-relativistic CR gyro time $t_{L,0,\rm cr} \equiv (m_{\rm cr}c)/(q_{\rm cr}\boldsymbol{B})$, where $m_{\rm cr}$ and $q_{\rm cr}$ are the CR mass and charge.

In the ideal MHD approximation, the 'feedback' force from dust grains and CRs appears simply in the gas momentum equation as an equal-and-opposite force as from gas on to dust +CRs:

$$\rho_{\rm gas}\left(\frac{\partial}{\partial t} + \boldsymbol{v}_{\rm gas}\cdot\nabla\right)\boldsymbol{v}_{\rm gas} = -\nabla P - \frac{\boldsymbol{B}\times(\nabla\times\boldsymbol{B})}{4\pi} - \int d^3\boldsymbol{v}_{\rm dust}\, f_{\rm dust}(\boldsymbol{x},\boldsymbol{v}_{\rm dust})\,\boldsymbol{a}_{\rm gas,dust}(\boldsymbol{v}_{\rm dust},...) - \int d^3\boldsymbol{v}_{\rm cr}\, f_{\rm cr}(\boldsymbol{x},\boldsymbol{v}_{\rm cr})\,\boldsymbol{a}_{\rm gas,cr}(\boldsymbol{v}_{\rm cr},...), \tag{6}$$

where $f_{\rm dust}(\boldsymbol{x},\boldsymbol{v}_{\rm dust})$ and $f_{\rm cr}(\boldsymbol{x},\boldsymbol{v}_{\rm cr})$ are the phase-space density distributions of dust and CRs, respectively. Non-Lorentz forces are integrated with a semi-implicit scheme and Lorentz forces using a Boris integrator, with the backreaction terms implemented in a manner that ensures manifest machine-accurate total momentum conservation. These methods have been detailed and extensively tested in Hopkins & Lee (2016), Lee, Hopkins & Squire (2017), Moseley, Squire & Hopkins (2019), Seligman et al. (2019), and Hopkins et al. (2020b).

Note that up to the detailed form of the gyro acceleration equation, the expressions for dust and gas evolution are functionally identical – indeed we can numerically think of the dust as a second, 'heavy' (low charge-to-mass, non-relativistic) CR species which also experiences drag, or think of the CRs as 'relativistic, drag-free grains.'

Finally, to avoid the Courant condition for the CR speed c leading to computationally impractical time-steps in our simulation, we adopt the reduced speed-of-light (RSOL) approximation by defining the RSOL $\tilde{c}$ in equation (5) $\tilde{c} < c$ (but still keeping $\tilde{c}$ much larger than other velocities in our simulation). As shown in Ji & Hopkins (2021), the particularly form of the RSOL implemented here, which simply modifies the CR acceleration by the power of $\tilde{c}/c$ and defines the CR advection speed over the (non-relativistic) grid to be $\boldsymbol{v}_{\rm cr}^{\rm advect} \equiv \partial\boldsymbol{x}_{\rm cr}/\partial t = (\tilde{c}/c)\,\boldsymbol{v}_{\rm cr}$, ensures that all steady-state properties of the CR distribution function (number, momentum, energy density, and pitch-angle distribution) are mathematically invariant to the choice of $\tilde{c}$. With this new implementation, we are able to simultaneously match the CR energy density, mass density, *and* momentum density of any desired initial configuration, and account for the 'correct' CR gyro-radius and backreaction forces which are also independent of the choice of $\tilde{c}$. This also means that throughout this paper when we refer to e.g. CR gyro-frequencies and other standard quantities, they have their usual meaning and values (i.e. unless otherwise specified, the RSOL $\tilde{c}$ does not enter our expressions here).

2.2 Simulation parameters and motivation

In what follows, we consider a system where dust grains are accelerated by some large $\boldsymbol{a}_{\rm ext,dust}$, for example from radiation pressure from e.g. a quasar or luminous starburst in their host galaxy, in low-density magnetized gas representative of e.g. the CGM or ionized ISM bubbles. In these cases the fastest growing of the dust RDIs are generally the 'aligned cosmic ray like' (so named because the eigenmode structure broadly resembles the Bell 2004 instability) or 'dust gyro-resonant' RDIs, which lead to rapid growth of parallel Alfvén waves which can scatter CRs. For the cases of interest, the external forces on the CRs $\boldsymbol{a}_{\rm ext,cr}$ are negligible.

Because this is a first study, to simplify the dynamics as much as possible and have a well-defined, resolved CR and dust gyro-radius, we consider just a single species of dust and single species of CRs. In reality of course there will exist a broad spectrum of dust sizes, with different charge and mass, e.g. and likewise spectrum of CR energies; but we will focus on parameters representative of the grains that contain most of the dust mass and dominate the 'feedback' force, as well as the CRs which dominate the CR energy density/pressure. We adopt a 3D box with a side-length of $L_{\rm box}$ and periodic boundary conditions, filled with initially homogeneous gas, dust, and CRs, with a uniform magnetic field whose initial direction defines the z axis ($\boldsymbol{B}_0 = |\boldsymbol{B}_0|\,\hat{z}$) and uniform velocity fields (i.e. the initial CR and dust distribution functions are taken to be δ-functions, though we discuss relaxing this below), and impose an isothermal ($\gamma = 1$) equation-of-state on the gas (motivated by typical cooling physics in the ISM/CGM). We adopt the same particle/cell numbers for gas, dust, and CRs, i.e. $N_{\rm gas} = N_{\rm dust} = N_{\rm cr} = N_{\rm 1D}^3$, where $N_{\rm 1D}$ is the 1D resolution along each sides of the simulation box, $N_{\rm 1D} = 64$ in our fiducial simulations (so the box contains 3×64^3 elements), and we also performed additional high-resolution simulations with $N_{\rm 1D} = 128$ for convergence tests. We initialize the dust drift velocity with its homogeneous equilibrium solution (see Hopkins et al. 2020b), the gas velocity $\boldsymbol{v}_{\rm gas} = 0$, and the CR velocity $\boldsymbol{v}_{\rm cr} = v_{\rm cr}\,\hat{z}$, defined below.

Even with these simplifications, writing the simulation parameters in units of the initial gas density $\rho_{\rm g}^0$, sound speed c_s^0 and box size $L_{\rm box}$, our simulations require we specify 10 dimensionless numbers: (1) The plasma beta $\beta \equiv (c_s/v_{\rm A})^2$, where $v_{\rm A} \equiv \boldsymbol{B}/\sqrt{4\pi\rho_{\rm gas}}$ is the Alfvén velocity; (2) The box-averaged dust-to-gas mass ratio $\mu_{\rm dust} \equiv \rho_{\rm dust}/\rho_{\rm gas}$; (3) The dust external acceleration $\bar{a}_{\rm dust} \equiv |\boldsymbol{a}_{\rm ext,dust}|L_{\rm box}/(c_s^0)^2$; (4) The dust 'size parameter' $\bar{\epsilon}_{\rm dust} \equiv \rho_{\rm dust}^i\epsilon_{\rm dust}/\rho_{\rm g}^0 L_{\rm box}$, which determines the grain drag forces; (5) The dust 'charge parameter' $\bar{\phi}_{\rm dust} \equiv 3Z_{\rm dust}e/(4\pi c\epsilon_{\rm dust}^2(\rho_{\rm gas}^0)^{1/2})$, which determines the grain charge-to-mass ratio and Lorentz forces; (6) The angle $\cos(\theta_{\rm dust}) \equiv \left|\hat{\boldsymbol{B}}_0\cdot\hat{\boldsymbol{a}}_{\rm ext,dust}\right|$ between initial B-field direction and external dust acceleration; (7) The CR-to-gas mass ratio $\mu_{\rm cr} \equiv \rho_{\rm cr}/\rho_{\rm gas}$ (or equivalently the CR number ratio $n_{\rm cr}/n_{\rm gas}$, since we are interested in CR protons); (8) The CR 'charge parameter' $\bar{\phi}_{\rm cr} \equiv q_{\rm cr}/(cm_{\rm cr})L_{\rm box}(\rho_{\rm gas}^0)^{1/2}$, which encodes the CR charge-to-mass ratio; (9) The angle $\cos(\theta_{\rm cr}) \equiv \left|\hat{\boldsymbol{B}}_0\cdot\hat{\boldsymbol{v}}_{\rm cr}\right|$ between the initial magnetic fields and CR velocity. (10) The initial CR Lorentz factor γ_L (or equivalently initial CR momentum $p_{\rm cr}$).

This forms an enormous parameter space, which is impossible to explore concisely. We therefore focus on one particular parameter set in this first study, motivated heuristically by the scenario proposed in Squire et al. (2021) and discussed above. Consider typical interstellar/intergalactic silicate or carbonaceous dust ($\rho_{\rm dust}^i \sim 1\,{\rm g\,cm^{-3}}$, with $\epsilon_{\rm dust} \sim 0.1\,\mu$m grains containing most of the mass, a standard ISM-like dust-to-gas ratio, and obeying the standard collisional+photoelectric charge law from e.g. Draine & Sutin 1987; Tielens 2005) and typical $\sim$1 GeV kinetic energy CRs which dominate the CR energy density ($\gamma_L \sim 2$ protons). These proposes in a medium with parameters typical of the warm (volume filling) CGM outside of a galaxy (gas temperature $T \sim 10^5$ K, density $n \sim 10^{-2}\,{\rm cm^{-3}}$, $|\boldsymbol{B}| \sim 0.1\,\mu$G, and CR-to-thermal pressure $P_{\rm cr}/P_{\rm therm} \sim$ a few; Ji et al. 2020). We wish to resolve some number

of CR gyro radii in our box, so set $L_{\rm box} \sim 10\, r_{L,\rm cr}$.[1] This gives the numerical parameters[2] $\beta \approx 2\times10^{3}$, $\mu_{\rm dust} \approx 0.01$, $\bar{\epsilon}_{\rm dust} \approx 10^{5}$, $\bar{\phi}_{\rm dust} \approx 1.6\times10^{6}$, $\mu_{\rm cr} \approx 3.6\times10^{-7}$, $\bar{\phi}_{\rm cr} \approx 1.3\times10^{5}$, $\gamma_L \approx 2$.[3] What remains is the external dust acceleration $\bar{a}_{\rm dust}$, which is the ultimate source of energy for the RDIs: a larger value of this parameter corresponds to more rapid RDI growth rates. Squire et al. (2021) considered supersonic dust drift velocities ($v_{\rm drift} \equiv |\boldsymbol{v}_{\rm dust} - \boldsymbol{v}_{\rm gas}|$), such that certain RDIs were excited, so we choose $\bar{a}_{\rm dust} = 1.2\times10^{-3}$ such that the initial equilibrium dust drift velocity is $v_{\rm drift} \approx 10\, c_s^0$ (safely supersonic).[4] As discussed in Hopkins & Squire (2018), Hopkins, Squire & Seligman (2020), and Squire et al. (2021), while this is intentionally a somewhat extreme choice, it is plausible given the observed radiative fluxes in CGM environments around superluminous sources such as quasars and starburst galaxies, e.g. at $\sim$10–100 kpc from a source with luminosity $\sim10^{12}$–$10^{13}\, L_\odot$.

It is easy to verify that under these conditions, Lorentz forces on dust grains strongly dominate over drag forces (by a factor of $\sim10^4$), as desired for our problem of interest, and that both CRs and dust have very similar gyro-radii, $\sim$0.6 au in the physical units above.

2.3 On the initial CR pitch angle distribution

Note that our initial condition for the CRs corresponds to all CRs having pitch angle =0 ($\mu = 1$), i.e. free-streaming directly down magnetic field lines at drift velocity $v_D^0 \sim c$ with the maximum-possible anisotropy in the CR distribution function. This is almost certainly unrealistic, but our purpose is to study how CRs would be scattered away from this anisotropy by dust, hence the choice.[5] However one consequence of this choice is that for the parameters above (with $(e_{\rm cr} v_D^0)/(e_B c) > 1$, where $e_{\rm cr}$ and e_B are the CR and magnetic energy densities), the non-resonant Bell instability would grow much faster than the CR resonant instability (Bell 1978; Haggerty, Caprioli & Zweibel 2019) and much faster than the RDIs (by a factor $\sim(\mu_{\rm cr}/\mu_{\rm dust})^{1/2}(v_D^0/v_{\rm dust}^0)(t_{L,\rm cr}^0/t_{L,\rm dust}^0)^{-1} \gg 1$). And indeed we have verified this directly in test simulations, which also allow us to confirm that, in code, both the non-resonant and resonant CR instabilities grow initially at their expected linear growth rates.

A more realistic initial condition would feature a close-to-isotropic CR distribution function, which would strongly suppress these instabilities relative to the RDIs, and we also consider this case below. However for a first simulation, in order to see how CRs would be scattered from an arbitrarily anisotropic distribution with $\mu = 1$ (which is particularly useful for understanding the scattering physics themselves), we consider the 'ultra-low CR density' or 'test-particle CR' limit. This amounts to to ignoring the CR feedback on the gas (equivalently, taking the CR number or energy density to be negligibly small), i.e. dropping the last term on the right-hand side in equation (6). Thus, CR scattering via self-induced instabilities cannot occur and we can cleanly isolate the effects of the RDIs. We study this as a test problem in Sections 3.1–3.3. After the system reaches a saturation state and CRs become more isotropized with $v_D \ll \tilde{c}$ (a more realistic 'initial condition' for the CRs), we turn on CR feedback and investigate its consequences in Section 3.4.

3 RESULTS

3.1 Time evolution and saturated states

Figs 1 and 2 shows plots of the dust grain projections, gas density fluctuations, gas velocity perturbations superposed with velocity streamlines, magnetic field strength superposed with field lines, and cosmic ray particle projections, viewed along the z-axis (the direction of the initial magnetic fields) and x-axis, respectively. We choose the snapshots at $t = 9.78\, t_{L,\rm dust}$, $10.22\, t_{L,\rm dust}$, $10.65\, t_{L,\rm dust}$, and $13.04\, t_{L,\rm dust}$, which are representative samples spanning between the end of the linear stage, the non-linear stage and the saturation stage. Dust grains are unstable to the RDI and non-linearly evolve into highly concentrated columns along the z-axis, which merge and form into fewer but thicker columns or sheets with time. At the saturation stage, all dust grains form into one single column in our simulation box. This is expected since all wavelengths are unstable to RDIs, and the RDI growth rates decrease with increasing wavelengths. Therefore, we see the merging of structures until the box-scale mode saturates. Compared to collisionless dust grains which are strongly clumped, gas is only weakly compressible, with density and velocity fluctuations at levels of $\sim$1 and 10 per cent, respectively. As shown in Figs 1 and 2, since field lines are strongly stretched by dust grains, magnetic fields are amplified by up to one order of magnitude from their initial values, and the regions of field amplification tightly trace the location of clustered dust. At the saturation stage, field lines become significantly distorted and wrap around columns of dust grains, with the magnetic tension force $\sim \boldsymbol{B}\times(\nabla\times\delta\boldsymbol{B})/4\pi$ balancing the driving force from the dust on the gas $\sim \rho_{\rm dust}\boldsymbol{a}_{\rm ext,dust}$ (Seligman et al. 2019). As illustrated in Fig. 3, the morphology of the gas density, dust distribution, and magnetic field strength are highly correlated, and the system reaches approximately dynamical equilibrium between the gas pressure $P_{\rm gas}$, the magnetic pressure $\sim|\boldsymbol{B}|^2/8\pi$ and the dust ram pressure $P_{\rm dust}$ (estimated as the dust momentum flux across the surface of the dust filament $\rho_{\rm dust} v_{z,\rm dust}\, v_{xy,\rm dust}$). Starting from a random distribution initially, CRs strongly react to RDI-induced magnetic field perturbations, being scattered and transiently becoming highly clustered together with the dust before scattering leads to their returning to a nearly random spatial distribution again at the saturation stage (but now with a nearly isotropic pitch angle distribution, as we show below). Initially the CRs react coherently small-scale modes (which have $\lambda \ll r_{L,\rm CR}$) because CRs initially have a perfectly coherent (δ function) distribution function and magnetic fields are distorted by the RDIs; but as the CRs scatter, these local 'concentrations' disperse.

Fig. 4 shows the probability density functions (PDFs) of densities (top) and velocities/Lorentz factor (bottom) for gas (left), dust (middle), and CRs (right). Density PDFs are obtained by mapping particle mass on to grids, and velocity/Lorentz factor PDFs are weighted directly by particle masses. Compared with gas densities which only vary by $\sim$20 per cent, the PDF of grain densities spans

[1] More precisely, we set $L_{\rm box} = \sqrt{N_{\rm 1D}}\, r_{L,\rm cr}$ such that each Larmor wavelength is resolved with $\sim\sqrt{N_{\rm 1D}}$ elements and the box contains $\sqrt{N_{\rm 1D}}$ Larmor wavelengths, which provides an optimal compromise for our purposes. For boxes with different resolution, we rescale the numerical parameters to correspond to fixed *physical* quantities (e.g. fixed gyro radii) while rescaling the box size to follow this relation. Here and throughout, we define the gyro-radius specifically as the gyro radius for an equivalent circular orbit, $r_{L,\rm cr} = |\boldsymbol{v}_{\rm cr}|\, t_{L,\rm cr}$.

[2] For our low-resolution $N_{\rm 1D} = 64$ boxes, the parameters that depend explicitly on $L_{\rm box}$ rescale to $\bar{\epsilon}_{\rm dust} \approx 1.5\times10^{5}$, $\bar{\phi}_{\rm cr} \approx 9\times10^{4}$, and $\bar{a}_{\rm dust} \approx 8.5\times10^{-4}$.

[3] We also set reduced speed of light to $\tilde{c} = 0.05\, c \approx 230 c_s^0$, ensuring it is larger than other speeds in the problem, but explicitly examine convergence with respect to this choice below.

[4] As there is no particular reason to expect alignment between $\boldsymbol{B}$ and $\boldsymbol{a}_{\rm ext,dust}$, we set $\theta_{\rm dust} = 45^\circ$, but this is largely a nuisance parameter.

[5] In contrast, because of drag, the only homogeneous stable equilibrium solution for the dust grains is uniform streaming at the equilibrium drift velocity, as we initialize.

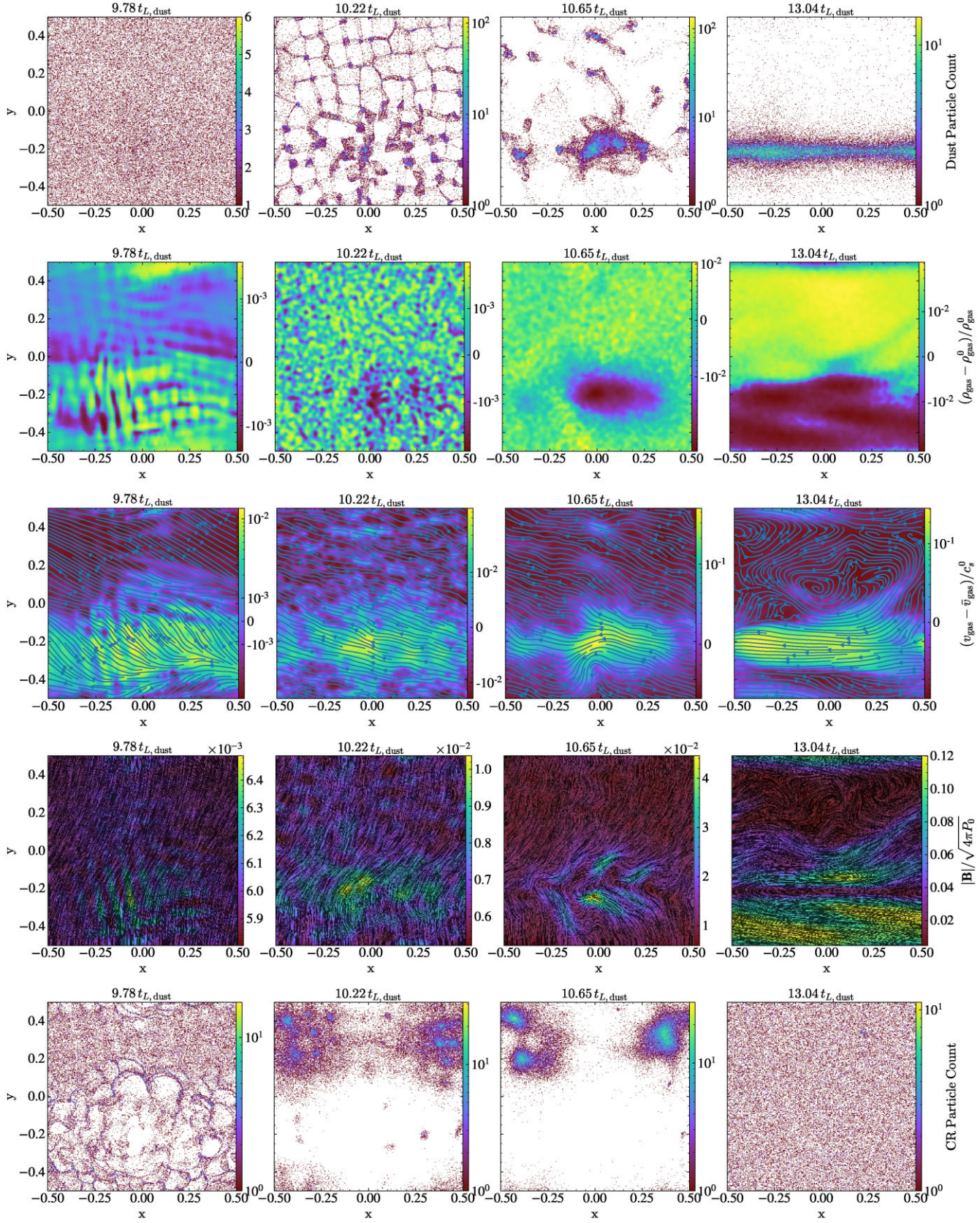

Figure 1. Plots of (from top to bottom) dust grain projections, gas density fluctuations, gas velocity perturbations superposed with velocity streamlines, magnetic field strengths superposed with field lines, and CR particle projections, at (from left to right) $t = 9.78\,t_{L,\mathrm{dust}}$, $10.22\,t_{L,\mathrm{dust}}$, $10.65\,t_{L,\mathrm{dust}}$, and $13.04\,t_{L,\mathrm{dust}}$, viewed along the z-axis (parallel with the direction of initial magnetic fields). Dust grains are unstable to the RDI and modes grow and merge until they saturate in a large box-scale sheet mode, which significantly distorts and amplifies magnetic fields. CRs strongly respond to and are scattered by dust-induced magnetic field irregularities.

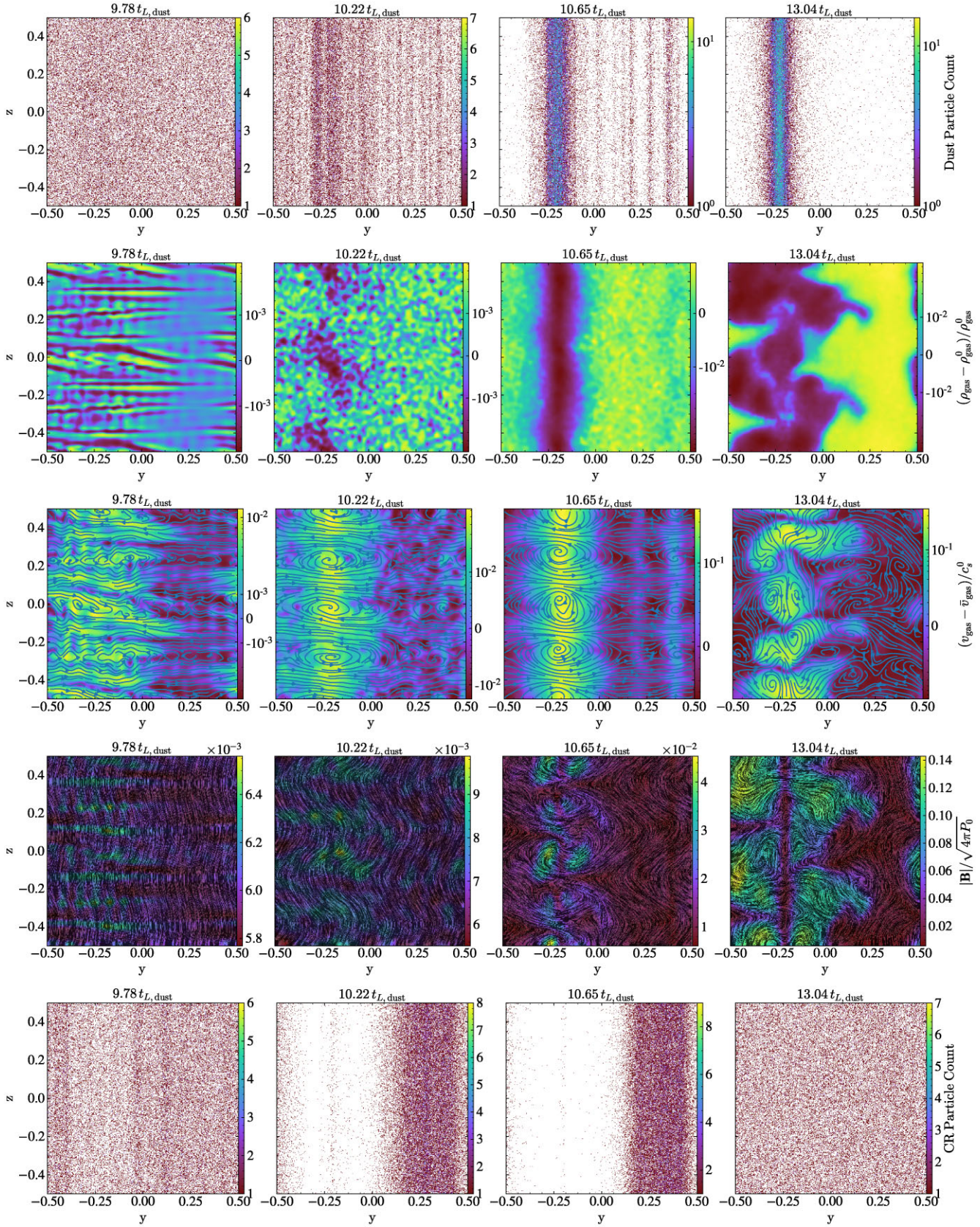

Figure 2. Plots as Fig. 1, but viewed along the x-axis (perpendicular to the direction of initial magnetic fields).

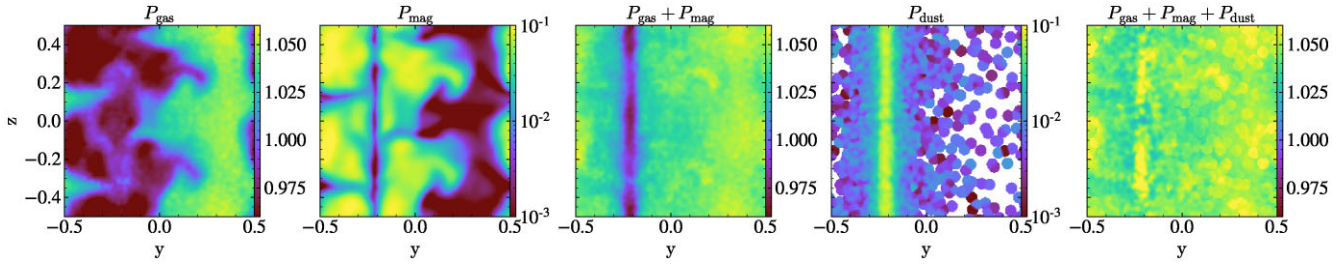

Figure 3. Slice plots of (from left to right) gas thermal pressure $P_{\rm gas}$, magnetic pressure $P_{\rm mag}$, the sum of gas thermal pressure and magnetic pressure $P_{\rm gas}+P_{\rm mag}$, dust ram pressure $P_{\rm dust}$ estimated as dust momentum flux across the surface of the dust filament $\rho_{\rm dust}v_{z,\rm dust}\,v_{xy,\rm dust}$, and the sum of all pressure terms $P_{\rm gas}+P_{\rm mag}+P_{\rm dust}$ in code units of $\rho^0_{\rm gas}(c^0_s)^2$, at the saturation stage when $t=13.04\,t_{L,\rm dust}$. The sum of pressure terms is nearly a constant spatially, indicating the system is roughly in pressure balance.

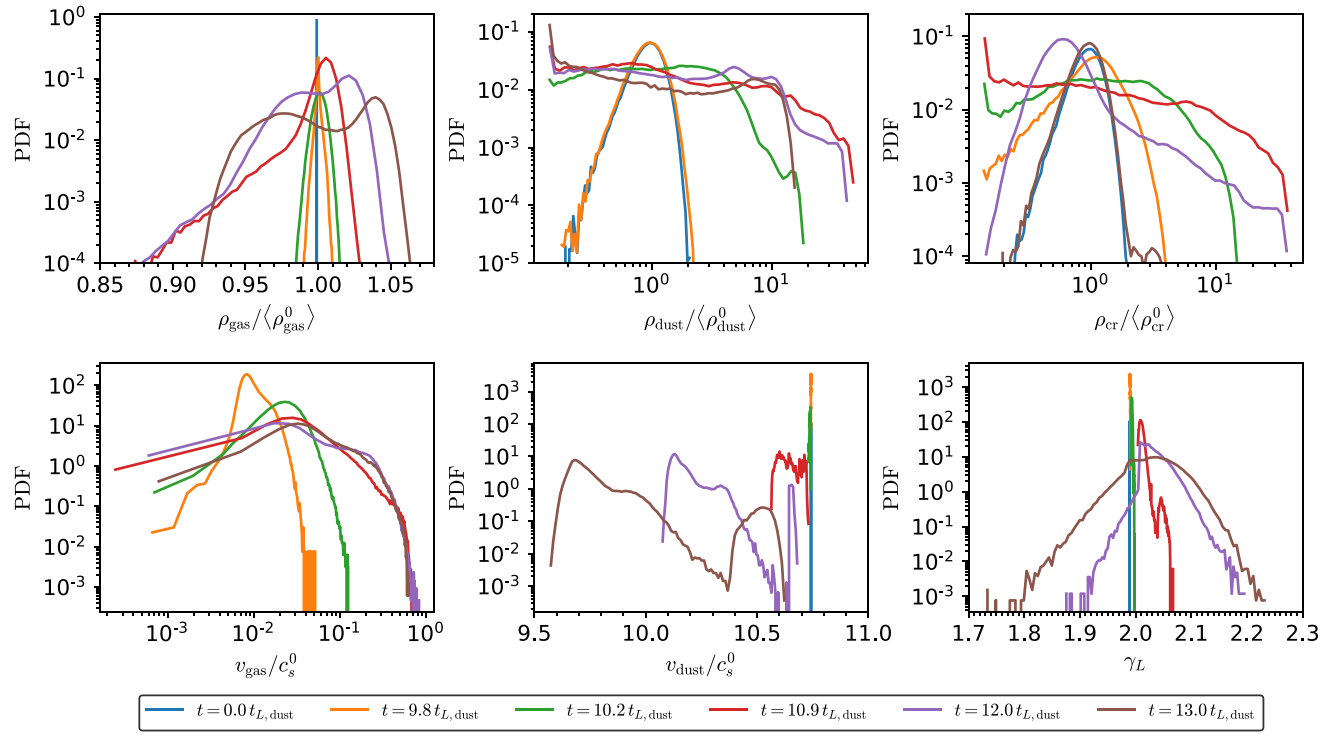

Figure 4. The density (top) and velocity/Lorentz factor (bottom) PDFs of gas (left), dust (middle), and CRs (right). Most PDFs feature a strong asymmetry. The density PDFs of dust and CRs span up to two orders of magnitude, while gas is only weakly compressible. Gas and dust grains are accelerated and decelerated, respectively, due to their momentum exchange, and the PDFs of CR Lorentz factor slightly broaden with time.

over two orders of magnitude and become highly non-Gaussian at the non-linear and saturation stages, with a flat tail extending to $\rho_{\rm dust}/\rho^0_{\rm dust}>10$ (similar to other pure-RDI simulations in, e.g. Seligman et al. 2019; Hopkins et al. 2020b). The relatively uniform PDF is qualitatively maintained in the high-resolution run, indicating that if there is a characteristic clumpiness, it's not yet being recovered by the simulation. The CR density PDFs are qualitatively similar to the dust density PDFs at the non-linear stage, as the initially coherent CRs are 'dragged' by the RDIs, while at the saturation stage when CRs become fully scattered, the CR density PDF recovers its initial Gaussian shape (for the reasons above). The gas velocity PDFs suggest that gas is significantly accelerated by dust feedback up to rms velocities $\langle v_{\rm gas}/c^0_s\rangle\sim10^{-2}$–$10^{-1}$. Dust grains are gently decelerated with time, and the velocity PDFs do not reach an equilibrium state by the end of the simulation. The CR Lorentz factor PDFs gradually broaden out with time, indicating CRs are mildly accelerated or decelerated by ~3 per cent during their interaction with local magnetic fields (i.e. some 'diffusive re-acceleration' effects with a non-zero CR momentum diffusion coefficient D_{pp}, as will be discussed in Section 3.3).

3.2 Growth rates versus linear theory

We next examine the amplification of magnetic fields $|\boldsymbol{B}_x|$, $|\boldsymbol{B}_y|$, and $|\boldsymbol{B}_z|$, and the growth of the CR velocity component perpendicular to local magnetic fields $v_{\perp,\rm cr}$ (normalized to the magnitude of total CR velocity $|\boldsymbol{v}_{\rm cr}|$). By defining the pitch angle θ as the angle between CR velocities and local magnetic field vectors, we see $v_{\parallel,\rm cr}/|\boldsymbol{v}_{\rm cr}|=\mu$ and $v_{\perp,\rm cr}/|\boldsymbol{v}_{\rm cr}|=(1-\mu^2)^{1/2}$, where $\mu\equiv\cos\theta$ is the pitch angle cosine and $v_{\parallel,\rm cr}$ the CR velocity component parallel with local magnetic fields. As shown in the top and middle panels of Fig. 5, $|\boldsymbol{B}_x|$, $|\boldsymbol{B}_y|$, and $v_{\perp,\rm cr}$ grow exponentially at almost the same growth rate until

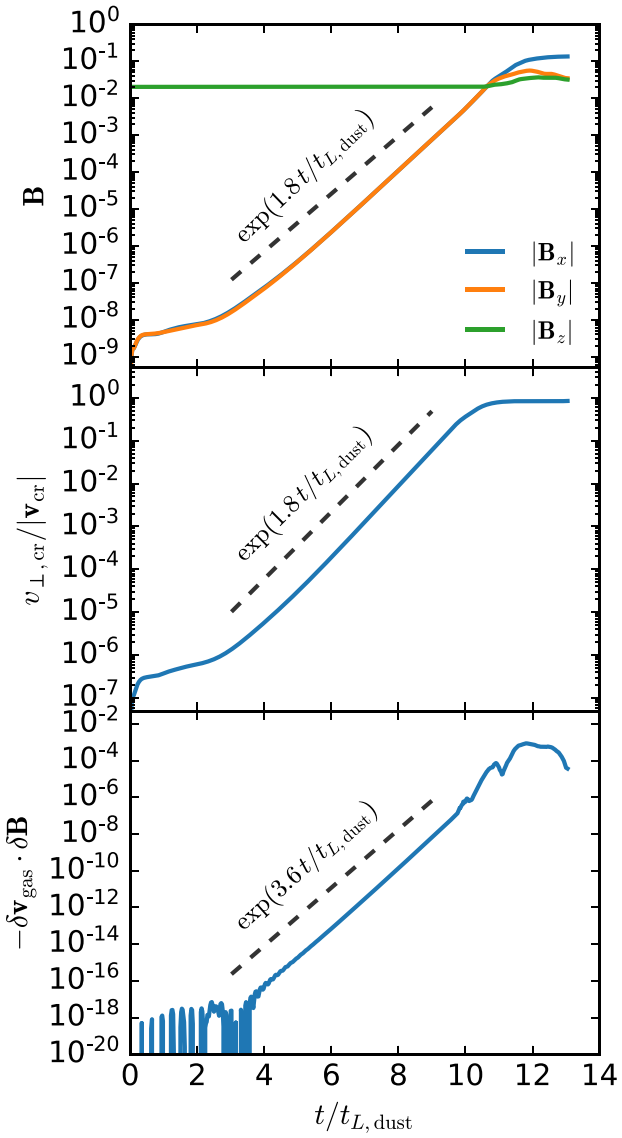

Figure 5. Time evolutions of averaged magnetic fields (top), the perpendicular component of CR velocity (middle), and the averaged negative gas cross helicity (bottom). Both the magnetic fields and the CR perpendicular velocity component follow almost the same analytically predicted growth rate (and the squared growth rate for the cross helicity since it is the dot product of velocities and magnetic fields), indicating a strong correlation between magnetic field fluctuations, Alfvén wave propagation and CR scattering.

they reach saturation at $t \sim 10\,t_{L,\mathrm{dust}}$. This indicates that, starting from highly anisotropic initial conditions with $v_{\perp,\mathrm{cr}}/|\boldsymbol{v}_{\mathrm{cr}}| = 0$, CRs are strongly scattered by increasingly distorted magnetic fields due to the development of the dust RDI.

To estimate the magnitude of CR bulk drift velocity, we measure the arithmetic mean values of the CR velocity components (the net drift velocity) over all CR particles at the saturation stage. We find that $\langle v_{\{xyz\},\mathrm{cr}}\rangle \sim \alpha c$ with α fluctuating between $\sim 10^{-4}$ and 10^{-2} with time, which is thus highly isotropic compared with the CR initial conditions of $\langle v_{x,\mathrm{cr}}\rangle^0 = \langle v_{y,\mathrm{cr}}\rangle^0 = 0$ and $\langle v_{z,\mathrm{cr}}\rangle^0 \sim c$. Although the magnitude of the 'residual' drift velocity $\sqrt{\Sigma^i_{xyz}\langle v_{i,\mathrm{cr}}\rangle^2}$ is of the same order of magnitude with $\langle v_{\mathrm{A}}\rangle$, given that we sample the CR distribution function with $\sim 10^6$ particles in our default simulations,

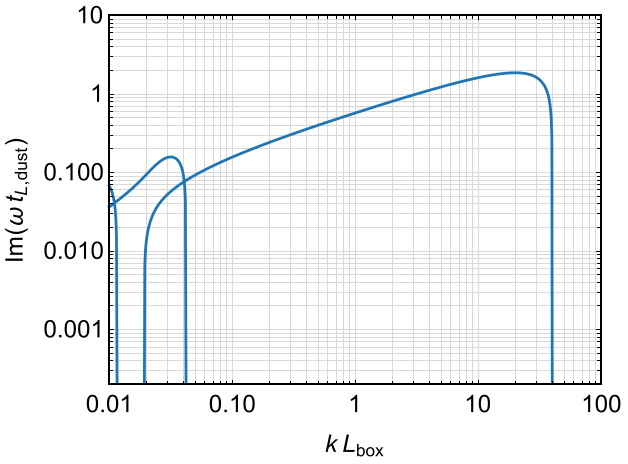

Figure 6. Analytical growth rates of RDI as a function of wavenumber $|\boldsymbol{k}|$, which perfectly predicts the growth rate measured directly from the simulation as shown in Fig. 5.

we caution that this range of α is precisely what we would expect from Monte Carlo sampling noise for an intrinsically uniform pitch-angle distribution. This sampling noise (which unfortunately converges slowly, as $N_{\mathrm{cr}}^{-1/2}$) dominates the 'residual' drift velocity here, thus we cannot draw a firm conclusion on the CR drift speed from direct measurement. However, there is still a way to investigate the CR drifting by Alfvén waves. As shown in the bottom panel of Fig. 5, the (negative) magnitude of the gas cross helicity $-\delta\boldsymbol{v}_{\mathrm{gas}}\cdot\delta\boldsymbol{B}$, which is related to the asymmetry of Alfvén waves, remains a single sign and grows exponentially with a squared RDI growth rate before saturating. This indicates that the propagation of the Alfvén waves excited by the RDIs is increasingly *unidirectional* (antiparallel to the large-scale magnetic fields in this case when the cross helicity is negative); therefore, the CRs must at least drift at $\sim v_{\mathrm{A}}$ by the Alfvén waves all propagating in one direction.

In Fig. 6, we plot the analytically predicted growth rates for our simulation parameters as a function of the wavenumber $|\boldsymbol{k}|$, for a specific mode angle of $\hat{\boldsymbol{k}}\cdot\hat{\boldsymbol{v}}_{\mathrm{dust}} = 0$.[6] We find that the growth rate measured from our simulation in Fig. 5 replicates the analytical solution well, with the growth rates peaking at wave numbers around $kL_{\mathrm{box}} \sim 10$–$40$. This corresponds to a fastest growing wavelength of $2\pi/k \sim 0.16$–$0.6L_{\mathrm{box}}$, which is somewhat consistent with the structures seen in Figs 1 and 2.

3.3 Pitch angle scattering and transport/scattering coefficients

Fig. 7 shows the time evolution of CR pitch angle PDFs (top) and the pitch angle diffusion coefficients $D_{\mu\mu}$ (bottom), which is defined as

$$D_{\mu\mu}(\mu_0, t_0) = \frac{\langle(\mu-\mu_0)^2\rangle}{2(\tilde{t}-\tilde{t}_0)} \quad \text{for } \tilde{t}-\tilde{t}_0 = \Delta\tilde{t} \text{ not too large,} \qquad (7)$$

where $\mu_0(\tilde{t}_0)$ and $\mu(\tilde{t})$ are initial and final pitch angle cosine (time), respectively, Δt is the integration time, and we trace the change of pitch angles for all CR particles over a short time interval to

[6]We explicitly verified that the mode angle of $\hat{\boldsymbol{k}}\cdot\hat{\boldsymbol{v}}_{\mathrm{dust}} = 0$, i.e. the wave vector and dust velocities are aligned or antialigned, gives the fastest growth rate, which is consistent with the findings in Seligman et al. (2019). Therefore, we only show the growth rates for this specific mode angle here. For a detailed description of calculating these growth rates (see Hopkins & Squire 2018).

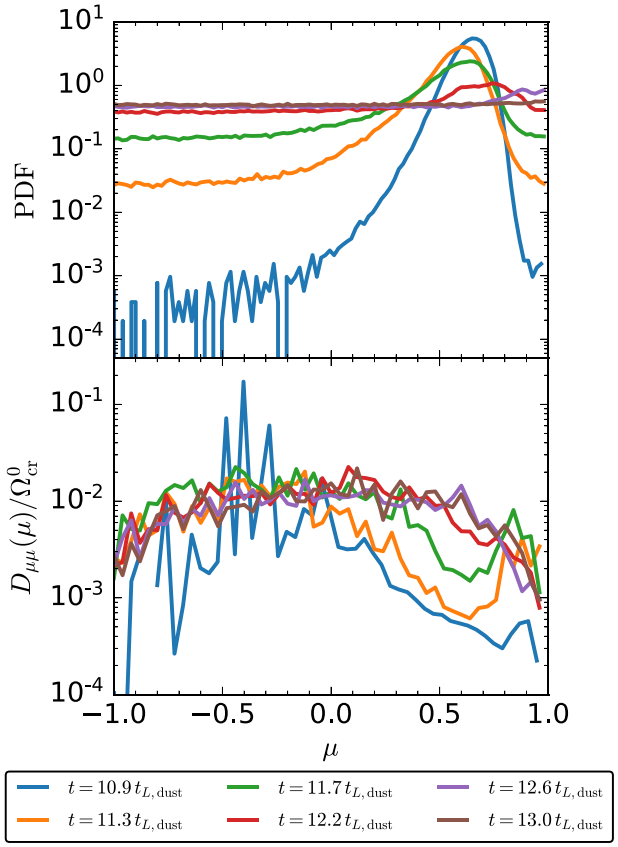

Figure 7. Time evolution of PDFs of the CR pitch angle cosine μ (top), and the CR pitch angle diffusion coefficient $D_{\mu\mu}$ (normalized by the initial CR gyro-frequency $\Omega^0_{\rm cr}$) as a function of the CR pitch angle cosine (bottom). At the saturation stage, CRs are fully isotropized with a uniform distribution of the pitch angle cosine, and the CR pitch angle diffusion coefficient features a flat profile around $\mu = 0$, without encountering the 90° pitch angle problem predicted by quasi-linear theories.

keep $(\mu - \mu_0)$ small, following e.g. Beresnyak, Yan & Lazarian (2011) and Xu & Yan (2013). Here $\tilde{t} \equiv (\tilde{c}/c)\,t_{\rm code}$ denotes the in-code time $t_{\rm code}$ multiplied by the factor $\tilde{c}/c$ to correct for the reduced speed of light (RSOL) approximation.[7] As shown in the top panel of Fig. 7, the distribution of CR pitch angles becomes uniform at the saturation stage, indicating that CRs are nearly isotropized, with typical $D_{\mu\mu} \sim 0.001$–$0.01\,\Omega_{\rm cr}$ (where $\Omega_{\rm cr} \equiv q_{\rm cr}\,|\boldsymbol{B}|/(\gamma_L m_{\rm cr} c)$ is the usual relativistic CR gyro-frequency).

[7]Specifically, as shown in Ji & Hopkins (2021), the implementation of the RSOL in our code is mathematically equivalent to taking the modified form of the general Vlasov equation for the CR distribution function to be: $(c/\tilde{c})\,\partial_t f_{\rm cr} + \boldsymbol{v}_{\rm cr}\cdot\nabla_{\boldsymbol{x}} f_{\rm cr} + \boldsymbol{F}_{\rm cr}\cdot\nabla_{\boldsymbol{p}} f_{\rm cr} = \partial_t f_{\rm cr}|_{\rm coll}$, i.e. rescaling the time derivative of the distribution function in the simulation frame by $\tilde{c}/c$. This ensures that once the CR distribution function reaches steady state, all effects of the choice of $\tilde{c} < c$ on its properties and on the plasma vanish, but also that the CRs 'respond' or evolve more slowly in time by a factor $\tilde{c}/c$ to perturbations – effectively rescaling the units of time 'as seen by' the CRs. This is precisely what allows us to uniformly increase the CR time-step by the factor $c/\tilde{c}$, which is the purpose of the RSOL, but this means in equation (7), we must rescale back to the 'true' $\Delta\tilde{t} = (\tilde{c}/c)\,\Delta t_{\rm code}$ to obtain the correct ($\tilde{c}$-independent) value of $D_{\mu\mu}$. We verify this explicitly in simulations with varied $\tilde{c}$ below.

For comparison, if we assume isotropic/grey scattering with the usual quasi-linear theory slab scattering expressions (Schlickeiser 1989), then we would expect the average value of $D_{\mu\mu}$ to be given by $\langle D_{\mu\mu}\rangle \sim (3\pi/16)\,\Omega_{\rm cr}\,|\delta\boldsymbol{B}|^2/|\boldsymbol{B}|^2$ (Zweibel 2013), where $\delta\boldsymbol{B}$ represents the magnitude of magnetic fluctuations on gyro-resonant scales. We see in Fig. 7 that our typical $D_{\mu\mu}$ values correspond to $|\delta\boldsymbol{B}| \sim 0.1\,|\boldsymbol{B}|$, which is roughly what we see in Figs 1–3 (in fact we see slightly larger overall magnetic fluctuations, but what matters here is the gyro-resonant, parallel component, so the effective $|\delta\boldsymbol{B}|^2$ entering the scattering-rate expressions we would expect to be reduced by a factor of ∼2–3). Thus, at least to order of magnitude or better, the typical scattering rate we see is consistent with quasi-linear theory expectations.

Examining $D_{\mu\mu}(\mu)$, we see that the CR pitch angle diffusion coefficients saturates at a smooth distribution as a function of μ (nearly μ-independent), which contradicts the usual prediction of $D_{\mu\mu}(\mu = 0) \sim 0$ from quasi-linear theory (e.g. Skilling 1971; Yan & Lazarian 2002). This prediction from quasi-linear theory is known as the 90° pitch angle problem, since $\mu = 0$ corresponds to an extremely short resonance wavelength which contains insufficient energy to scatter CRs away from the 90° pitch angle, and thus CRs might be naively expected to become 'trapped' at $\theta = 90°$ without being fully isotropized (e.g. Giacalone & Jokipii 1999; Felice & Kulsrud 2001). However, in our simulation, since the RDI-induced magnetic field perturbation $\delta B/B$ can grow up to a few 10^{-1}, CRs can be scattered across the 90° pitch angle and become isotropic without any difficulty, suggesting the dust RDI is efficient in exciting small-scale parallel Alfvén waves and confine CRs on ∼au scales. Previous studies have suggested that resonance broadening due to non-linear wave-particle interactions (e.g. Yan & Lazarian 2008; Bai et al. 2019) or mirror scattering (e.g. Felice & Kulsrud 2001) might help to avoid the 90° pitch angle problem, which may be occurring in our simulations as well.

With this, we can further estimate the CR parallel diffusion coefficient $\kappa_\parallel$ from our simulation in standard fashion (Earl 1974):

$$\kappa_\parallel \approx \frac{1}{8}\int_{-1}^{1} d\mu\,\frac{v_{\rm cr}^2(1-\mu^2)^2}{D_{\mu\mu}(\mu)}. \tag{8}$$

Calculating this numerically in the saturation stage, we obtain $\kappa_\parallel \sim 1.7\times10^4\,c_s^0\,L_{\rm box} \sim 700\,c\,r_{L,\rm cr} \sim 0.7\times10^{27}\,(|\boldsymbol{B}|/0.1\,\mu{\rm G})^{-1}\,{\rm cm^2\,s^{-1}}$, i.e. a factor of ∼1000 larger than the Bohm limit. This value is significantly lower than typical values of $\kappa \sim 10^{29-30}\,{\rm cm^2\,s^{-1}}$ inferred from Solar system measurements or γ-ray observations of Local Group galaxies (Blasi & Amato 2012; Amato & Blasi 2018; Chan et al. 2019; Hopkins et al. 2020), suggesting that dust-induced scattering near quasars or superluminous galaxies can lead to strong CR confinement.

In Fig. 4, we clearly see that there is also some non-zero diffusion in CR momentum space. In quasi-linear theory again, the effective CR momentum-space diffusion coefficient D_{pp} is trivially related (to leading order in $\mathcal{O}(u/c)$, where u represents the background plasma velocities) to the pitch-angle-averaged $\langle D_{\mu\mu}\rangle$ as

$$\langle D_{pp}\rangle \sim \chi\,\frac{p_{\rm cr}^2 v_{\rm A}^2}{v_{\rm cr}^2}\,\langle D_{\mu\mu}\rangle, \tag{9}$$

where the factor of χ depends on the CR distribution function, and is ∼1/3 for nearly isotropic CRs (Hopkins et al. 2021a). Measuring $\langle D_{pp}\rangle$ either 'directly' (for an ensemble of CRs, as we estimated $D_{\mu\mu}$) or 'indirectly' (by measuring the broadening of the PDF of $p_{\rm cr}$ or γ_L in Fig. 4 and comparing to an analytic diffusion solution), we confirm that the momentum-space diffusion coefficient estimated

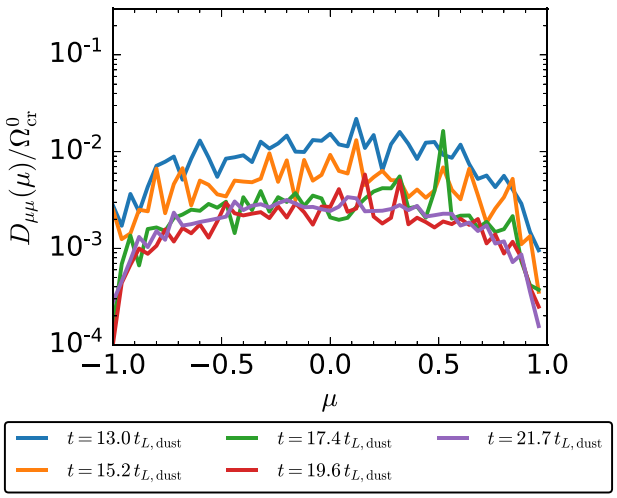

Figure 8. Time evolution of the CR pitch angle diffusion coefficient $D_{\mu\mu}$ (normalized by the initial CR gyro-frequency $\Omega^0_{\rm cr}$) as a function of the CR pitch angle cosine μ, as the bottom panel of Fig. 7 but with CR feedback turned on. CR feedback lowers the CR pitch angle diffusion coefficient by roughly one order of magnitude, and the 90° pitch angle problem does not occur either.

numerically is within tens of percent of the value one would infer from simply inserting our measured $\langle D_{\mu\mu}\rangle$ into equation (9).

3.4 Pitch angle scattering with CR feedback

We now investigate how CR feedback (backreaction from CRs on to gas and magnetic fields) modifies the our previous findings. After the CR population becomes nearly isotropized at $t \sim 13 t_{L,\rm dust}$, we continue evolving our simulation but now enable CR feedback. Since at this stage the CR drift velocity is much less than the speed of light ($v_D \ll c$), and the CR 'initial conditions' are more physically realistic, the CR non-resonant instability does not grow rapidly and dominate the simulation behaviour (as it artificially would if we began from $v_D \approx c$ with CR feedback included). Almost all of our qualitative conclusions and the behaviors (in saturation) of gas, CR, and dust density fields remain qualitatively similar after turning on this backreaction term, but quantitatively, there is some effect. Specifically in Fig. 8, we plot the time evolution of the CR pitch angle diffusion coefficient $D_{\mu\mu}$ as a function of the CR pitch angle cosine μ, after re-enabling the CR feedback. With CR feedback present, $D_{\mu\mu}$ decreases somewhat (though it conserves the functional form of $D_{\mu\mu}(\mu)$) until saturating at a value systematically lower by a factor $\sim$4 compared to that without CR feedback. This in turn implies factor $\sim$4 higher parallel diffusion coefficients. This is still more than sufficient to keep the CRs isotropized and strongly confined (and the 90° pitch-angle problem still does not appear), but it is not a negligible difference.

Physically, we showed in Section 3.3 that the scattering rates followed approximately the quasi-linear theory expectation, $D_{\mu\mu} \propto |\delta\boldsymbol{B}|^2/|\boldsymbol{B}|^2$. Thus a factor $\sim$4 suppression of $D_{\mu\mu}$ by CR backreaction corresponds to a factor of $\sim$2 suppression of $\delta\boldsymbol{B}$ on gyro-resonant scales. Indeed, we can directly verify that after we turn on the CR feedback the fluctuations in the magnetic field are damped by roughly this factor. If the fluctuations are predominantly driven by the RDIs, then this change in their saturation amplitudes is not surprising: recall from Section 2.2, when we turn on backreaction (i.e. account for finite CR pressure effects on gas), we assume a fairly large CR pressure relative to thermal pressure, $P_{\rm cr} \sim 5\,P_{\rm thermal}$ (with both $P_{\rm cr}$ and $P_{\rm thermal}$ much larger than magnetic pressure). Thus if we saturate as described in Section 3.1 with the perturbations driven by the RDIs (ultimately powered by the dust 'ram pressure' or acceleration force per unit area $P_{\rm dust}$) compensated by gas thermal *plus* CR pressure, then we expect $|\delta\boldsymbol{B}|^2$ to be a factor of a few lower in saturation (from the increase in the *total* thermal+magnetic+CR background pressure). Effectively, the background medium becomes 'stiffer' against perturbation by the dust.

From the view point of the standard quasi-linear theory wherein one assumes linear growth of scattering modes compensated by wave damping setting the quasi-steady-state scattering rates, with the CR feedback turned on, the backreaction on the RDI from the CR pressure plus the magnetic tension leads to stronger damping, and thus less CR confinement as found in the simulations. Quasi-linear theories also predict that the CR feedback can generate small-scale Alfvén waves via the CR gyro-resonant and non-resonant instabilities, i.e. the CR 'self-confinement' modes which add linearly with the RDI driven perturbations and thus *increase* the CR confinement. However, this is in opposite to the decrease of the CR confinement in our simulations, because CRs are highly isotropic in the saturation stage, thus the CR-excited Alfvén waves and their resulting CR confinement are negligible. But admittedly, it is plausible to imagine that if there is a continuous driving of the background CR gradients, the growth rates of Alfvén waves from dust and CRs do add linearly when they both have drifts and small densities, and we might see the enhancement of the CR confinement, as quasi-linear self-confinement theories predicted.

3.5 Convergence tests

Although previous studies have investigated how simulations of just the RDIs (Moseley et al. 2019; Seligman et al. 2019; Hopkins et al. 2020b) or just CRs depend on resolution, those simulations did not combine these physics nor investigate the same range of scales and parameters as we do here. Therefore, we consider a 'high-resolution' simulation with $N_{\rm gas} = N_{\rm dust} = N_{\rm cr} = N_{\rm 1D}^3 = 128^3$. Note that since we enforce $r_{L,\rm dust}/L_{\rm box} = \sqrt{N_{\rm 1D}}$, the high-resolution run with doubled 1D resolution fits a factor-of-$\sqrt{2}$ larger number of Larmor wavelengths along each side of the simulation domain, and resolves each Larmor wavelength with $\sqrt{2}$ times more elements.

Fig. 9 shows projections of dust grains, slices of magnetic field strength superposed with field lines and projections of CR particles along the z-axis for the high-resolution simulation. The high-resolution run is qualitatively similar to the low-resolution run shown in Fig. 1, but contains smaller scale structures as expected. At the saturation stage, the high-resolution run contains two large-scale coherent structures of dust columns and magnetic vortices, in contrast to the single sheet-like structure in the low-resolution run. This is likely because the high-resolution run contains more Larmor wavelengths and thus it simulates a larger domain in real physical units. The time evolution of the magnetic fields and the perpendicular CR velocity in the high-resolution run are shown in Fig. 10, where the growth rate is almost identical to the low-resolution run. Thus the linear growth rates of the relevant modes are not measurably dependent on resolution, and they agree well with analytic theory; moreover the final properties (widths) of the PDFs are similar in both cases. Of greatest interest, the values of $D_{\mu\mu}$ and (correspondingly) $\kappa_\parallel$ and D_{pp} differ by less than 5 per cent in the high-resolution run. Thus it appears that the key results here are not sensitive to resolution. However, we caution that it is only possible to numerically resolve a tiny fraction of the interesting dynamic range

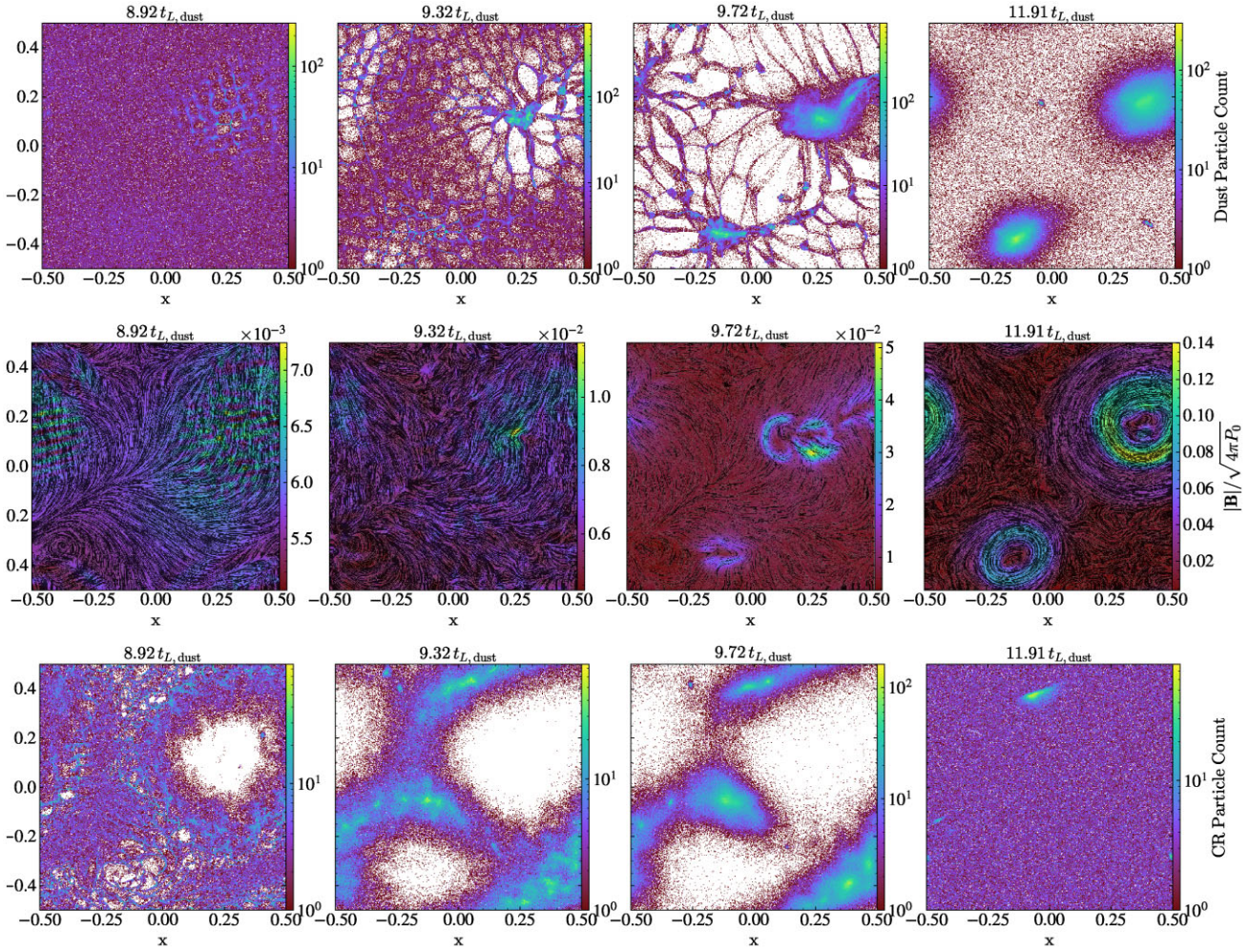

Figure 9. Plots of dust grain projections (top), magnetic field strengths superposed with field lines (middle), and CR particle projections (bottom), as Fig. 1, but from the high-resolution simulation. The morphology of dust grains, magnetic fields, and CRs in the high-resolution run is qualitatively similar with those in the fiducial run, but exhibits more detailed small-scale structures and contains more large-scale coherent structures (since the domain size of the high-resolution run is effectively larger – see the text for a full explanation).

(let alone effects like turbulent cascades or field-line wandering from large-scale dynamics, which operate on orders-of-magnitude larger scales), so this should be taken with some caution.

We also examine the numerical convergence with respect to the RSOL by varying $\tilde{c}$ over a factor of $\sim$5. For standard-resolution runs with $\tilde{c} = (0.02,\ 0.05,\ 0.1)\,c$, we find qualitatively identical behaviour in all properties studied here, with the numerically estimated in-saturation parallel diffusion coefficients $\kappa_{\parallel} \sim (700,\ 700,\ 600)\,c r_{L,\mathrm{cr}}$, respectively – i.e. nearly invariant to $\tilde{c}$. Note there is a (very weak) hint that $\kappa_{\parallel}$ may decrease with increasing $\tilde{c}$ here, perhaps owing to slightly stronger confinement at higher $\tilde{c}$ perhaps because with lower $\tilde{c}$ the CRs response may slightly artificially lag the RDI growth rates; but if we extrapolate to $\tilde{c} = c$ by fitting our results, the resulting inferred $\kappa_{\parallel}$ is only decreased by $\sim$40 per cent, a rather small correction compared to other theoretical uncertainties here (e.g. the effect of backreaction discussed below).

3.6 Discussion: damping and saturation scalings

Owing to our limited numerical resolution and MHD-PIC assumptions (where the plasma is treated as an MHD fluid), our simulations do not include certain plasma processes that can also damp Alfvén waves, such as ion-neutral or Landau damping. Ion-neutral damping is not likely relevant under conditions of interest for our problem here (e.g. diffuse, warm, highly illuminated CGM), as the expected neutral fractions are vanishingly small. But Landau damping could be non-negligible, in principle. If we consider e.g. the usual non-linear Landau damping rate with $\Gamma \sim (\sqrt{\pi}/4)\,c_s\,k\,(k_{\perp}^2/k_{\parallel}^2) \sim (\sqrt{\pi}/8)\,c_s\,k\,(|\delta\boldsymbol{B}|^2/|\boldsymbol{B}|^2)$, then at the scale where the RDI growth rate is maximized ($\sim r_{L,\mathrm{cr}}$) the implied Landau damping rate (given the $|\delta\boldsymbol{B}| \sim 0.1\,|\boldsymbol{B}|$ we see) is generally $\sim$10 per cent of the RDI growth rate in Fig. 6. That suggests it may not be negligible, but it is also unlikely to qualitatively change the behaviours here, if included. However, the simulations do, given the finite resolution, have non-zero numerical dissipation which happens (coincidentally) to be similar in magnitude to Landau damping: given a standard numerical MHD dissipation rate in GIZMO which scales as $\sim \Delta x\,c_s\,k^2 \sim c_s\,k\,(k\,\Delta x)$ (where Δx is the effective grid resolution for the MHD, and the prefactor depends on the specific numerical problem and details of the method, see Hopkins & Raives 2016), then for $k \sim 1/r_{L,\mathrm{cr}} \sim 1/(10\,\Delta x)$ this is roughly similar in magnitude to the physical Landau damping. Of course, other mechanisms could in principle contribute to damping including interactions with extrinsic

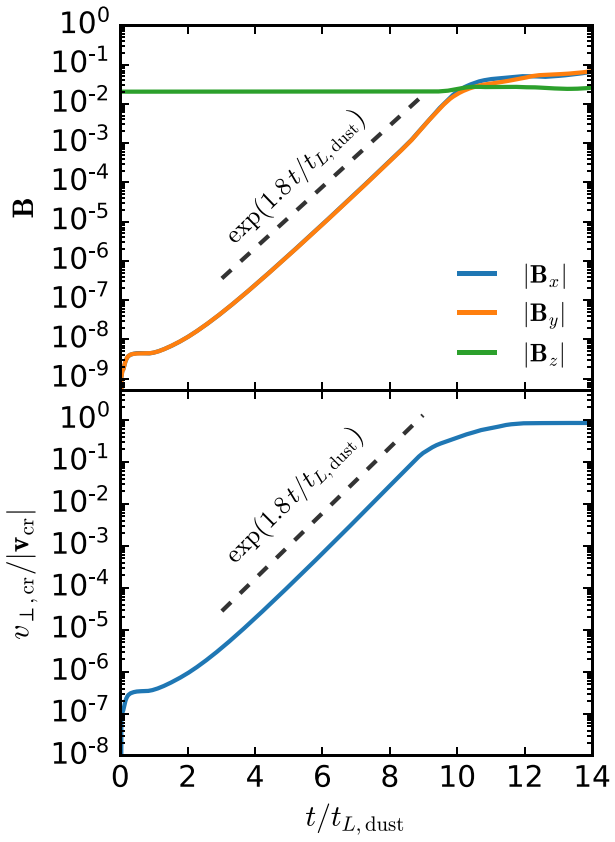

Figure 10. Time evolution of averaged magnetic fields (top) and the perpendicular component of of CR velocity, as Fig. 5, but from the high-resolution simulation. The exponential growth rate is almost identical to that in the fiducial run (Fig. 5), suggesting different resolutions do not significantly alter the results of our simulations.

turbulence (Farmer & Goldreich 2004), which we cannot capture owing to our limited range of scales. Dust itself could act as a damping mechanism in some circumstances (Squire et al. 2021) but the conditions where this would occur are dramatically different from those here.

These limitations in physics, finite resolution, and simulation box size preclude making detailed statements regarding the saturation mechanisms of the RDI across a broader parameter space. However, the fact that we see roughly isotropic $D_{\mu\mu}$ following approximately the expected quasi-linear scaling with $|\delta\boldsymbol{B}|/|\boldsymbol{B}|$ gives us some confidence that the CR scattering rates induced by the RDI should indeed scale with the saturation amplitude of $\delta\boldsymbol{B}$. And even if the saturation mechanism is uncertain, some broad conclusions are robust. For example, based on their idealized RDI-only simulations, Hopkins et al. (2020b) discuss two possible saturation mechanisms, the first being balance between magnetic tension and dust ram pressure as discussed in Section 3.1, the second being a scenario where the crossing time of the RDI-generated modes ($\sim\delta\boldsymbol{v}_{\mathrm{gas}}/\lambda$) becomes faster than the RDI growth time, producing non-linear dissipation. Non-linear Landau damping is another potential saturation mechanism, limiting $\delta\boldsymbol{B}$ when the damping becomes faster than linear RDI growth rates. Squire et al. (2021) consider yet another saturation scenario, assuming a Kraichnan (1965)-like damping via self-interactions (which gives a damping rate akin to non-linear Landau but with c_s replaced by the Alfvén speed). Crucially, the 'driving' in all of these scenarios scales with the dust-to-gas ratio $f_{\mathrm{dust-gas}}$ and force/acceleration/drift velocity on the grains (which appear in both the dust ram pressure and RDI growth rates). This is proportional to the incident radiation flux F_{rad}. Combining these estimates for the saturation $\delta\boldsymbol{B}$ with the usual scalings for gyro radii and scattering rates we obtain, for *any* of the saturation scenarios above, a scattering rate which scales dimensionally as $D_{\mu\mu} \propto f_{\mathrm{dust-gas}}\, F_{\mathrm{rad}}^{0.7-1.5}\, |\boldsymbol{B}|^{-(0.8-3)}$ (with a weaker residual dependence on gas density and/or temperature, and the exact power-law scaling depending on the saturation model). In other words, there is a qualitatively robust prediction that with lower dust-to-gas-ratios and/or incident radiative fluxes and/or stronger magnetic fields, the confinement of CRs by dust become weaker. All else equal, in order for the scattering rate from the dust RDIs to drop to below that inferred for Milky Way ISM gas (and thus become relatively unimportant), the factor $\sim f_{\mathrm{dust-gas}}\, F_{\mathrm{rad}}$ would need to be $\sim$1000 times smaller than the value we assume to motivate our tests. So for there to be 'too little dust,' the metallicity or dust-to-metals ratio would need to be 1000 times lower than ISM values (which seems unlikely at least at low cosmological redshifts, even in the CGM, given the observations reviewed in Section 1, which suggest this factor is perhaps something like $\sim$10 times lower than in the ISM). But more plausibly, the incident flux could easily be 1000 times smaller, if for example the galaxy is a typical Milky Way-like or smaller dwarf galaxy with a star formation rate of $\ll 10\,\mathrm{M}_{\odot}\,\mathrm{yr}^{-1}$ and has negligible AGN luminosity (i.e. galaxy luminosity $\lesssim 10^{10}\,\mathrm{L}_{\odot}$) or the dust is at $\gg 100$ kpc from the host. The magnetic field dependence is also interesting: it suggests these instabilities and ensuing confinement would be easier to excite in the distant CGM or IGM (where nano-Gauss fields are expected), but may be suppressed in denser, more highly ionized superbubbles near to galaxies.

4 CONCLUSIONS

In this paper, we investigate the impact of the dust RDIs on cosmic ray scattering, by performing the first numerical simulations of MHD-dust-CR interactions, where the charged dust and CR gyro-radii on $\sim$au scales are fully resolved. Since this is a first study, we consider just one special case, where we might anticipate efficient dust-induced CR confinement, as compared to more typical Solar-neighbourhood-like ISM conditions. We focus on *one* regime of the RDIs, specifically conditions where the 'cosmic ray-like' RDIs are rapidly growing and can produce 'diffusive' dust behaviour (see Hopkins et al. 2020b), which as speculated in Squire et al. (2020) could in turn lead to dust-induced CR confinement. This type of RDI requires particular conditions to dominate: $v_{\mathrm{dust}} \gg v_{\mathrm{A}}$, plasma $\beta \gg 1$, low gas density and high grain charge, so the dust drag force is substantially subdominant to the Lorentz force. These conditions could arise in, e.g. the CGM around quasars or luminous galaxies. We suspect that different RDIs might have different effects on CR scattering, which is a subject for future study. Under these conditions, we find that small-scale parallel Alfvén waves excited by the RDIs efficiently scatter CRs and significantly enhance CR confinement. Therefore, dust-induced CR scattering can potentially provide a strong CR feedback mechanism on $\sim$au scales.

We first explore the ultralow CR density limit by ignoring CR feedback to the gas. Dust quickly becomes unstable to the RDIs and forms high-density columns and sheets, until growth saturates around $\sim$10 times the dust Larmor time $t_{L,\,\mathrm{dust}}$. The density and velocity PDFs of both gas-and-dust grains show strong asymmetry, where the dust density spans over two orders of magnitude, while the gas is only slightly compressible with $\sim$10 per cent density fluctuations. Perpendicular magnetic field components are exponentially amplified by the RDI, with the growth rates predicted by analytical solutions.

Initially perfectly streaming CRs are strongly scattered by magnetic field fluctuations, with the growth rate of the perpendicular CR velocity component (to local magnetic fields, $v_{\perp,\rm cr}/|\boldsymbol{v}_{\rm cr}|$, or $\sqrt{1-\mu^2}$) equaling the growth rate of magnetic fields. At the saturation stage, the CRs are isotropized with a near-uniform distribution of the pitch angle cosine μ, and the CR pitch angle diffusion coefficient $D_{\mu\mu}(\mu)$ is nearly independent of pitch-angle μ (in particular around $\mu = 0$). There is no 90° pitch angle problem in our simulations. The scattering rate is in order-of-magnitude agreement with the usual quasi-linear theory expectation $D_{\mu\mu} \sim \Omega_{\rm cr}\,|\delta\boldsymbol{B}|^2/|\boldsymbol{B}|^2$, with the large $|\delta\boldsymbol{B}|^2/|\boldsymbol{B}|^2 \sim 10^{-3} - 10^{-2}$ on gyro-resonant scales driven by the dust RDIs (in part because the dust has broadly similar gyro-radii to the CRs, under these types of conditions). The numerically calculated CR parallel diffusion coefficient is ∼500–1000 times the Bohm value: sufficient for strong confinement of the CRs.

When the system reaches saturation and CRs become close to isotropic (with the CR drift velocity $v_D \ll \tilde{c}$), we turn on CR feedback to the gas and study its consequences. We find that with CR feedback, the CR pitch angle diffusion coefficient $D_{\mu\mu}$ decreases by a factor of ∼4 (and thus this slightly reduces CR confinement). This owes to the fact that the large assumed CR pressure (several times larger than thermal+magnetic) suppresses the saturation amplitude of the magnetic field fluctuations $\delta\boldsymbol{B}$ induced by the RDIs by a modest factor ∼2, and the scattering modes are thus damped more by backreaction on the RDIs from the CR pressure, in addition to the magnetic tension. Since CRs in the saturation stage are highly isotropic, the quasi-linear self-confinement theory which predicts *higher* scattering rates due to CR-excited Alfvén waves is *not* applicable here, unless there exists a continuous driving of CR gradients.

We finally stress that several caveats apply to our study. (1) As a first experiment, we picked one particular initial condition to investigate an interesting case, which is plausible for some conditions as noted above but should not be considered typical everywhere. There exist a variety of RDIs which can have totally different behaviours in different circumstances (Hopkins et al. 2020b) and indeed, under some conditions dust might even have the opposite effect, acting as a wave-damping mechanism and reducing the confinement of CRs (Squire et al. 2020). (2) Although we perform a small resolution study, our simulations are still limited in resolution and dynamical range. Even for a single grain size, the RDIs are unstable at all spatial wavelengths, so it is impossible to encompass their complete dynamic range (let alone global scales of structure or extrinsic turbulence, which are vastly larger than our box sizes). (3) We do not include any explicit wave-damping processes. While we do not expect appreciable ion–neutral damping in environments of interest (as the neutral fractions are negligible), Landau damping could be important, as could damping from a turbulent cascade, and these could reduce the efficacy of confinement. However at least for the extreme parameters considered here, it is unlikely these would significantly reduce the scattering rates. (4) Our periodic boxes neglect large-scale ($\gg L_{\rm box}$) CR pressure gradients ($\nabla P_{\rm cr}$) which act as a source/driving term for super-Alfvénic CR drift. (5) For simplicity, we consider only one grain size+charge and one CR energy+species, rather than a full spectrum of grain sizes and CR energies. In future work it will be particularly interesting to see how a full spectrum of both modifies the dynamics here, as a broad range of gyro-radii overlap and different gyro-resonant modes can interact non-linearly and even linearly (when CRs+dust+gas are all combined), via their backreaction on the gas.

With these limitations in mind, we consider this study to be a *proof of concept*, showing that CR dust–gas interactions might indeed be very important in some astrophysical conditions. For instance, this mechanism might be able to resolve some of the incompatibility between CR confinement models and observations by preventing CR 'runaway' (Hopkins et al. 2021a), at least under certain conditions investigated in this study. Considerable work remains to map out the parameter space, include additional physics, and understand the macroscopic consequences of confining CR–dust interactions (for either CRs themselves or for galaxy/CGM evolution). Nevertheless, the simulations here clearly argue that these effects are worth studying in detail.

ACKNOWLEDGEMENTS

SJ thanks E. Quataert for helpful discussions, and the referee for constructive comments which improve this manuscript. SJ is supported by a Sherman Fairchild Fellowship from Caltech, the Natural Science Foundation of China (grants 12133008, 12192220, and 12192223) and the science research grants from the China Manned Space Project (No. CMS-CSST-2021-B02). Support for JS was provided by Rutherford Discovery Fellowship RDF-U001804 and Marsden Fund grant UOO1727, which are managed through the Royal Society Te Apārangi. Support for PFH was provided by NSF Research Grants 1911233 and 20009234, NSF CAREER grant 1455342, NASA grants 80NSSC18K0562, *HST*-AR-15800.001-A, JPL 1589742. Numerical calculations were run on the Caltech compute cluster 'Wheeler,' allocations FTA-Hopkins/AST20016 supported by the NSF and TACC, and NASA HEC SMD-16-7592. We have made use of NASA's Astrophysics Data System. Data analysis and visualization are made with PYTHON 3, and its packages including NUMPY (Van Der Walt, Colbert & Varoquaux 2011), SCIPY (Oliphant 2007), MATPLOTLIB (Hunter 2007), and the yt astrophysics analysis software suite (Turk et al. 2010).

DATA AVAILABILITY

The data supporting the plots within this article are available on reasonable request to the corresponding author. A public version of the GIZMO code is available at http://www.tapir.caltech.edu/~phopkins/Site/GIZMO.html.

REFERENCES

Amato E., Blasi P., 2018, Adv. Space Res., 62, 2731
Bai X.-N., Stone J. M., 2010, ApJ, 722, L220
Bai X.-N., Caprioli D., Sironi L., Spitkovsky A., 2015, ApJ, 809, 55
Bai X.-N., Ostriker E. C., Plotnikov I., Stone J. M., 2019, ApJ, 876, 60
Bell A., 1978, MNRAS, 182, 147
Bell A. R., 2004, MNRAS, 353, 550
Beresnyak A., Yan H., Lazarian A., 2011, ApJ, 728, 60
Blasi P., Amato E., 2012, JCAP, 2012, 010
Buck T., Pfrommer C., Pakmor R., Grand R. J. J., Springel V., 2020, MNRAS, 497, 1712
Butsky I. S., Quinn T. R., 2018, ApJ, 868, 108
Carballido A., Stone J. M., Turner N. J., 2008, MNRAS, 386, 145
Chan T., Kereš D., Hopkins P., Quataert E., Su K., Hayward C., Faucher-Giguère C., 2019, MNRAS, 488, 3716
Deng H., Mayer L., Latter H., Hopkins P. F., Bai X.-N., 2019, ApJS, 241, 26
Draine B. T., Sutin B., 1987, ApJ, 320, 803
Earl J., 1974, ApJ, 193, 231
Evoli C., Gaggero D., Vittino A., Di Bernardo G., Di Mauro M., Ligorini A., Ullio P., Grasso D., 2017, JCAP, 2, 015
Farber R., Ruszkowski M., Yang H.-Y., Zweibel E., 2018, ApJ, 856, 112
Farmer A. J., Goldreich P., 2004, ApJ, 604, 671
Felice G. M., Kulsrud R., 2001, ApJ, 553, 198

Giacalone J., Jokipii J., 1999, ApJ, 520, 204
Grudić M. Y., Guszejnov D., Hopkins P. F., Offner S. S. R., Faucher-Giguère C.-A., 2021, MNRAS, 506, 2199
Guo F., Oh S. P., 2008, MNRAS, 384, 251
Haggerty C., Caprioli D., Zweibel E., 2019, Proc. Sci., Hybrid Simulations of the Resonant and Non-Resonant Cosmic Ray Streaming Instability. SISSA, Trieste, PoS(ICRC2019)279
Hennawi J. F. et al., 2010, ApJ, 719, 1672
Holcomb C., Spitkovsky A., 2019, ApJ, 882, 3
Hopkins P. F., 2015, MNRAS, 450, 53
Hopkins P. F., 2016, MNRAS, 462, 576
Hopkins P. F., 2017, MNRAS, 466, 3387
Hopkins P. F., Lee H., 2016, MNRAS, 456, 4174
Hopkins P. F., Raives M. J., 2016, MNRAS, 455, 51
Hopkins P. F., Squire J., 2018, MNRAS, 479, 4681
Hopkins P. F. et al., 2020, MNRAS, 492, 3465
Hopkins P. F., Squire J., Seligman D., 2020, MNRAS, 496, 2123
Hopkins P. F., Squire J., Butsky I. S., Ji S., 2021a, preprint (arXiv:2112.02153)
Hopkins P. F., Squire J., Chan T., Quataert E., Ji S., Keres D., Faucher-Giguère C.-A., 2021b, MNRAS, 501, 4184
Hunter J. D., 2007, Comput. Sci. Eng., 9, 90
Ji S., Hopkins P. F., 2021, MNRAS, preprint (arXiv:2111.14704)
Ji S. et al., 2020, MNRAS, 496, 4221
Ji S., Kereš D., Chan T., Stern J., Hummels C. B., Hopkins P. F., Quataert E., Faucher-Giguère C.-A., 2021, MNRAS, 505, 259
Jóhannesson G. et al., 2016, ApJ, 824, 16
Johansen A., Youdin A., Mac Low M.-M., 2009, ApJ, 704, L75
Jokipii J. R., 1966, ApJ, 146, 480
Kraichnan R. H., 1965, Phys. Fluids, 8, 1385
Kulsrud R., Pearce W. P., 1969, ApJ, 156, 445
Lee M. A., Völk H. J., 1973, Astrophys. Space Sci., 24, 31
Lee H., Hopkins P. F., Squire J., 2017, MNRAS, 469, 3532
Martin C. L., Scannapieco E., Ellison S. L., Hennawi J. F., Djorgovski S., Fournier A. P., 2010, ApJ, 721, 174
McKinnon R., Vogelsberger M., Torrey P., Marinacci F., Kannan R., 2018, MNRAS, 478, 2851
Ménard B., Scranton R., Fukugita M., Richards G., 2010, MNRAS, 405, 1025
Moseley E. R., Squire J., Hopkins P. F., 2019, MNRAS, 489, 325
Oliphant T. E., 2007, Comput. Sci. Eng., 9, 10
Pakmor R., Pfrommer C., Simpson C. M., Springel V., 2016, ApJ, 824, L30
Pan L., Padoan P., Scalo J., Kritsuk A. G., Norman M. L., 2011, ApJ, 740, 6
Peek J., Ménard B., Corrales L., 2015, ApJ, 813, 7
Ruszkowski M., Yang H.-Y. K., Zweibel E., 2017, ApJ, 834, 208
Salem M., Bryan G. L., Corlies L., 2016, MNRAS, 456, 582
Schlickeiser R., 1989, ApJ, 336, 243
Seligman D., Hopkins P. F., Squire J., 2019, MNRAS, 485, 3991
Skilling J., 1971, ApJ, 170, 265
Squire J., Hopkins P. F., 2018, ApJ, 856, L15
Squire J., Hopkins P. F., Quataert E., Kempski P., 2021, MNRAS, 502, 2630
Strong A. W., Moskalenko I. V., 2001, Adv. Space Res., 27, 717
Su K.-Y. et al., 2020, MNRAS, 491, 1190
Tielens A. G. G. M., 2005, The Physics and Chemistry of the Interstellar Medium. Cambridge University Press, Cambridge, UK
Tielens A., McKee C., Seab C., Hollenbach D., 1994, ApJ, 431, 321
Turk M. J., Smith B. D., Oishi J. S., Skory S., Skillman S. W., Abel T., Norman M. L., 2010, ApJS, 192, 9
Van Der Walt S., Colbert S. C., Varoquaux G., 2011, Comput. Sci. Eng., 13, 22
van Marle A. J., Casse F., Marcowith A., 2019, MNRAS, 490, 2249
Xu S., Yan H., 2013, ApJ, 779, 140
Yan H., Lazarian A., 2002, Phys. Rev. Lett., 89, 281102
Yan H., Lazarian A., 2008, ApJ, 673, 942
Zweibel E. G., 2013, Phys. Plasmas, 20, 055501

This paper has been typeset from a TEX/LATEX file prepared by the author.